

The Color between the Dots

Peter G. Engeldrum*

Imcotek, Winchester, Massachusetts 01890

Abstract

Reflectance models of halftone images, such as the Murray-Davis equation for monochrome and the Neugebauer equations for color, generally are not satisfactory predictors of average reflectance or tristimulus values (TSVs), even when used with the Yule-Nielsen n -factor. CIE colorimetric measurements of halftone dots and the paper between the dots for cyan, magenta, and yellow wax thermal transfer halftone images showed that the CIE tristimulus values of the dots and the paper are a function of the printed dot fractional area. The dependence of dot and paper TSVs on area was empirically modeled by a power function. Model exponents between 0.264 and 0.392 were found for the paper, and the exponents ranged from about 10^{-13} to 0.401 for the dot. A key finding was that the paper TSVs are linear mixtures of paper and a limiting TSV, whereas the dot TSVs are linear mixtures of the same limiting value and the solid-area TSVs. The limiting TSV was determined from the spectral product of the paper and the colorant layer transmittance. The empirical models for paper and dot TSVs were used to predict the X, Y, and Z TSVs for cyan, magenta, and yellow halftone patches. CIE L*a*b* coordinates were predicted to within an average color difference of 2.95 for the cyan and magenta, and 4.49 for the yellow, both within the variability of the particular printer.

Introduction

Reproduction of pictures via halftone techniques has been with us for 140 years. Fox Talbot is credited with the first optical halftone screen as we know it today.¹ Halftoning is about the only way to synthesize tones for binary, 1-bit imaging systems. The basic idea of a halftone is to vary the area covered by imaging material (colorant) to create the illusion of tones or lightness levels. Key to the success of the illusion is the assumption that the human visual system will spatially integrate over a sufficient area, thus creating the desired tones.

The Yule-Nielsen “ n ” Value.

Prediction of tone via the measurement of reflectance or density has a long history. In 1936, Murray² published an equation that linked together the average reflectance with the reflectance of the paper, the ink, and the area covered by the ink, as shown in Eq. 1.

$$R_{avg} = area R_{ink} + (1 - area)R_{paper} \quad (1)$$

Equation 1 worked adequately for halftone transparencies with well-defined dots (hard dots), but was soon found wanting for halftone images on paper. Generally

the average reflectance of halftones measured darker than predicted by Eq. 1. Fifteen years later, Yule and Neilsen³ suggested that the essential problem was the lateral scattering (diffusion) of light within the bulk of the paper. To correct the average measured reflectance for the paper scattering they suggested a modification of Eq. 1 by incorporating a factor—the now-famous n value. Equation 2 is known as the Yule-Nielsen equation.

$$R_{avg}^{1/n} = area R_{ink}^{1/n} + (1 - area)R_{paper}^{1/n} \quad (2)$$

In their original work Yule and Nielsen (Y-N) found that the n value varied from about 1 to 3 and depended on the spatial frequency ruling of the halftone screen and on paper properties. More recently Pearson⁴ has suggested that an average n value of 1.7 should be satisfactory when the actual n value is unknown.

A model governing halftone color printing was put forth in 1937 by H. E. Neugebauer.⁵ In its simplest form this model can be derived by assuming that three colorant layers, cyan, magenta, and yellow, composed of halftone images, are randomly superimposed. Each colorant layer is assumed to follow Eq. 1, so the three-colorant sandwich is the point-by-point product of the layers. Desktop color printers often use the so-called dot-on-dot halftone printing method, which has a different color formation model.⁶ The accuracy of the equations modeling halftone color printing are dependent upon the scattering of light within the paper. There are numerous reports of the effectiveness of incorporating a Y-N n value in various ways.⁷⁻¹⁰

Today, the Y-N equation continues to find adherents in studies of halftone color reproduction.^{5,7,11} This can probably be traced to the fact that the equation simply captures, more or less accurately, complex phenomena associated with halftone images on paper.

Other efforts at understanding the light-scattering phenomenon continue. In 1953 Callahan¹² reported a more sophisticated model, which was the basis of detailed analysis provided by Lehbeck,¹³ Ruchdeshel and Hauser,¹⁴ and Maltz¹⁵ decades later. Callahan's contribution was the recognition of what was later called the paper spread function by Yule, Howe, and Altman.¹⁶ Unfortunately, Callahan concluded that the influence of the paper spread function was of minor importance relative to all the other errors in color printing. A year later, 1954, Clapper and Yule¹⁷ revisited the issue with a ray-trace analysis that considered multiple internal reflections of light within the paper.

Although the observed effect of light scatter within the paper has long been recognized, there is a paucity of measurements available in the literature. There are no microcolorimetric measurements of which the author is

aware. Ottinen and Saarelmala¹⁸ offered some measurements with their theory, but with only two points per halftone configuration tested, the actual relationships of dot and paper reflectance with dot area remains unclear.

The practical motivation for understanding the colorimetric properties of halftone images is to build color correction methods and tables for desktop color printers. Optimum color image quality will remain illusive until practical approaches are developed that incorporate the effect of paper spread function. It seems clear that Neugebauer⁵ or dot-on-dot⁶ color reproduction theory will not be fundamentally accurate, even with an n -factor correction, because they do not account for the variation in dot and paper colorimetry as a function of the amount of colorant in the halftone image. Theories that exist^{13-15,18} for the spatial reflectance distribution of halftone images can be extended to color images. What is missing is the experimental data to verify these theories and additional simplified approaches for implementation. This report describes a step in that direction.

Experimental

Samples

A series of halftone patches of cyan, magenta, and yellow were printed on a color wax thermal transfer PostScript printer, with 300 dots/in. addressability, using paper recommended by the printer manufacturer. The halftone cell pattern was of the dispersed type with 12 dots/side. This halftone cell configuration provided a maximum of 144 colorant levels in an area of approximately 1×1 mm, equivalent to 25 halftone cells/in. Dispersing the addressable dots within the halftone cell produces an image structure different from that of the conventional or clustered dot.

A total of 256 1-cm-square patches were printed. Using the commands in the PostScript page description language, fine control of the fractional area covered by the colorant could be achieved. The wax thermal printer provided a simple image structure consisting of a wax colorant layer on top of highly calendered, but "plain," paper. A wax thermal printer was selected because it permits a simple image structure—a transparent "filter" layer on top of a simple paper structure.

Measurements

Several measurements of the cyan, magenta, and yellow halftone images were required for this investigation: (1) the microspectral reflectance of the dots and paper between the dots; (2) macrospectral reflectance of halftone tints; (3) dot spectral transmittance; and (4) the actual dot area occupied by dots.

The microspectral reflectances of the colored wax dot and the unprinted paper in the center of the halftone cell were measured. These reflectances were obtained by configuring a PhotoResearch PR-650 (Chatsworth, CA) spectroradiometer with a high-magnification "video" lens. Illumination was provided by an annular fiber optic ring set at a distance to provide 45/0 degree geometry. The spectral reflectance and transmittance were obtained by dividing the spectral radiance obtained from the halftone image by the spectral radiance obtained from a reference white.

For transmittance measurements the no-sample radiance was the reference. Both the dot-plus-paper and paper alone were measured, and the paper spectral transmittance was divided into the paper-dot spectral measurements to yield the dot transmittance. For the reflectance data a ceramic plaque of known spectral reflectance provided the reference. In this mode of operation the absolute calibration of the radiometer was unknown, but the objective was to derive a ratio, so the absence of the absolute calibration did not contribute any spectral error.

A circle of 0.13 mm diameter defined the area for the microspectral measurements. The finite size of the measuring aperture limited the minimum dot size and the minimum paper area. For large-area (macro) measurements of the halftone images, the 12-mm, $f/2.7$ lens provided with the spectroradiometer was used. This yielded the average spectral reflectance over a circle 10 mm in diameter. Illumination was identical to that used for the microspectral reflectance measurements.

Spectral data are provided by the spectroradiometer at every 4 nm, but the instrument has an 8-nm bandwidth over the spectral range 380-730 nm. The 4-nm data was linearly interpolated to every 10 nm over the same spectral range to use ASTM E308 standard tables for CIE XYZ tristimulus calculations for illuminant F2 (cool-white fluorescent).

Developing relationships of dot and paper tristimulus values (TSVs) in terms of area covered required knowledge of the actual fractional area printed by the wax thermal printer. There is no guarantee that the actual total area of printed dots within the halftone cell is equal to the area requested by the software. Printed area is a function of printer setup, thermal history, and any "calibration" or look-up tables that alter the relationship between the fractional areas (tone reproduction). The actual printed fractional areas were obtained using a photometrically calibrated monochrome CCD video camera and a PC-based 8-bit frame grabber (512 h \times 480 v pixels). The procedure consisted of displaying an image of at least one halftone cell on a color monitor and coding a threshold "gray" value in yellow. The threshold was adjusted manually by keyboard entry that altered the red, green, and blue look-up tables until the yellow color defined the boundaries of the halftone dots. A histogram of the halftone image was determined and served as the basis for the average area measurements. The fraction of the pixels in the histogram below the threshold was used as the measured fractional area.

Results

The data points in Figs. 1-3 show the measured micro X , Y , and Z CIE TSVs for the paper between the cyan, magenta, and yellow dots. In Figs. 4-6 are the microtristimulus data for the cyan, magenta, and yellow dots.

With the measuring aperture of 0.13 mm defined by optical configuration, the size of the paper "hole" and the size of the smallest dot that could be measured were limited. Thus the paper micro-TSVs at a fractional area of 1.0 are not directly measured values. They are measured indirectly, using the following logic. Assume that the spectroradiometer is looking through a hole in the

colorant layer that is small compared to the extent of the paper optical spread function. Under this condition there is complete scattering within the paper “under” the hole. The amount of incident light through the hole is negligible due to its small size, so there is no direct contribution of the incident flux. All the flux comes through the adjacent colorant layer and is reflected by the paper. In this case the measured microspectral reflectance is just the product of the macrospectral transmittance of the wax colorant layer (filter) and the macrospectral reflectance of the paper. This is the limiting case for the paper reflectance when the fractional area covered approaches 1.0, as shown by the data plotted in Figs. 1-3.

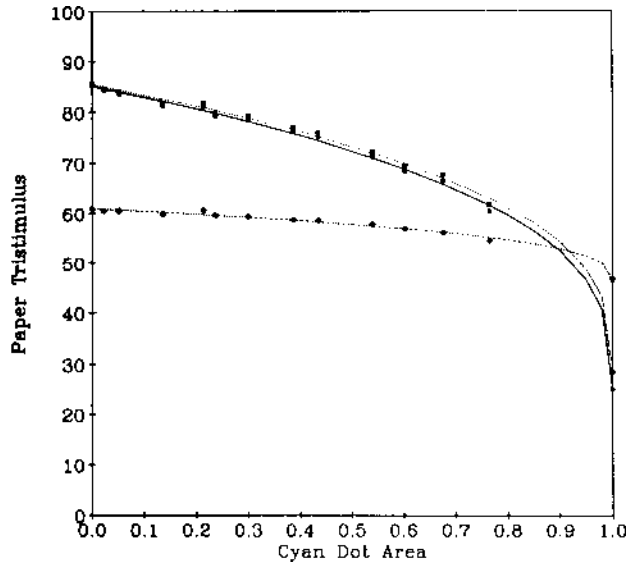


Figure 1. CIE X, Y, and Z TSVs for the paper between the cyan dots as a function of printed fractional area. The dot \equiv X, the square \equiv Y, and the diamond \equiv Z. The lines through the points are model predictions.

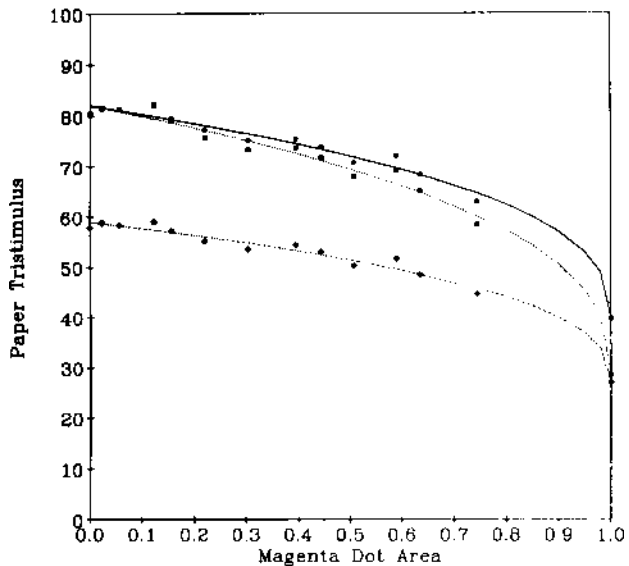


Figure 2. CIE X, Y, and Z TSVs for the paper between the magenta dots as a function of printed fractional area. The dot \equiv X, the square \equiv Y, and the diamond \equiv Z. The lines through the points are model predictions.

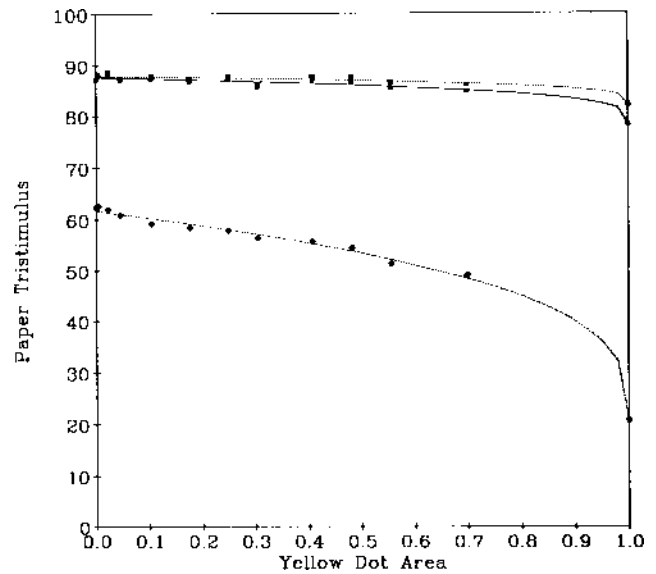


Figure 3. CIE X, Y, and Z TSVs for the paper between the yellow dots as a function of printed fractional area. The dot \equiv X, the square \equiv Y, and the diamond \equiv Z. The lines through the points are model predictions.

Similar logic provides the limiting microspectral reflectance of the dot as the dot area approaches zero. For dots the flux “under” the dot is just the paper macroreflectance, because the dot is so small that it does not spectrally modulate the incident flux. Remarkably, the limiting macrospectral reflectance for the dot approaching zero area is the same as for the hole: the paper macroreflectance times the spectral macro-transmittance of the dot.

It is possible to validate the above limiting cases by plotting the CIE chromaticity coordinates, $x = X/(X + Y + Z)$ and $y = Y/(X + Y + Z)$ of the data in Figs. 1-6, as is shown in Fig. 7. Essentially, each plot of the three colorants consists of two straight line segments. The central convergence point is the chromaticity coordinate of the paper, and the points close to that point are the chromaticities of the paper between the dots. The cluster of points at the extremes of the lines are the dot chromaticities. In the middle is an isolated point, the limiting case for a dot of zero area and a hole of 1.0 fractional area. This figure readily shows that the chromaticities of the paper between the dots lie along a line connecting the uncovered paper with the limiting dot-area chromaticity. Dot chromaticities show the same general result—the yellow is particularly clear.

Another result comes from the property of the chromaticity diagram: linear tristimulus mixtures plot as straight lines.¹⁹ Thus the data from Fig. 7 indicate that the TSVs of both the paper and, at least, the yellow dots can be formulated as two different linear tristimulus mixtures. This result is expected on the basis of the complete scattering of light in the paper. Complete scattering “averages” the incident light from two sources, the paper and the limiting value.

TABLE I. Parameter Summary for Power Function Fits to the Data in Figs. 1-6 using Eqs. 3a-b

		Paper			Dots		
		$T_{paper}-T_{limit}$	T_{limit}	p	$T_{limit}-T_{solid}$	T_{limit}	p
Cyan	X	60.15	24.90	0.343	10.25	24.96	0.141
	Y	57.01	28.39	0.346	11.42	28.45	0.139
	Z	14.56	46.45	0.373	5.76	46.56	0.401
Magenta	X	42.44	39.58	0.388	10.05	39.68	0.363
	Y	53.53	28.54	0.388	10.63	28.62	0.247
	Z	32.01	26.97	0.392	10.36	27.05	0.268
Yellow	X	9.44	78.19	0.275	1.28	78.19	0
	Y	5.86	85.05	0.264	0.682	82.05	0
	Z	40.95	20.72	0.328	10.82	20.78	0.308

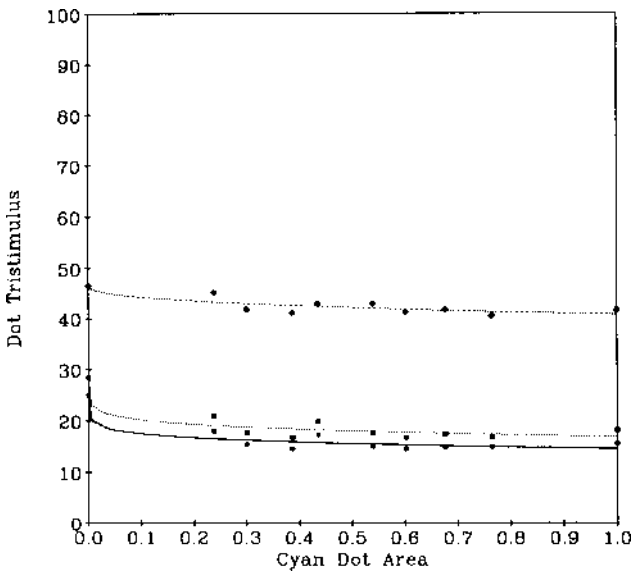


Figure 4. CIE X, Y, and Z TSVs for the cyan dots as a function of printed fractional area. The dot \equiv X, the square \equiv Y, and the diamond \equiv Z. The lines through the points are model predictions.

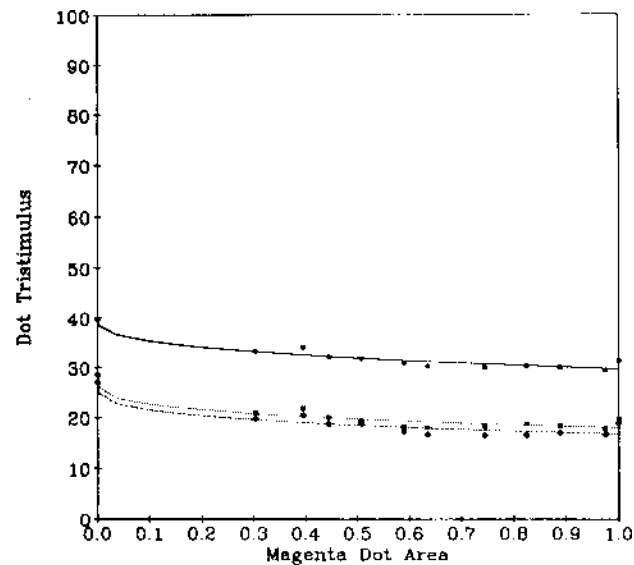


Figure 5. CIE X, Y, and Z TSVs for the magenta dots as a function of printed fractional area. The dot \equiv X, the square \equiv Y, and the diamond \equiv Z. The lines through the points are model predictions.

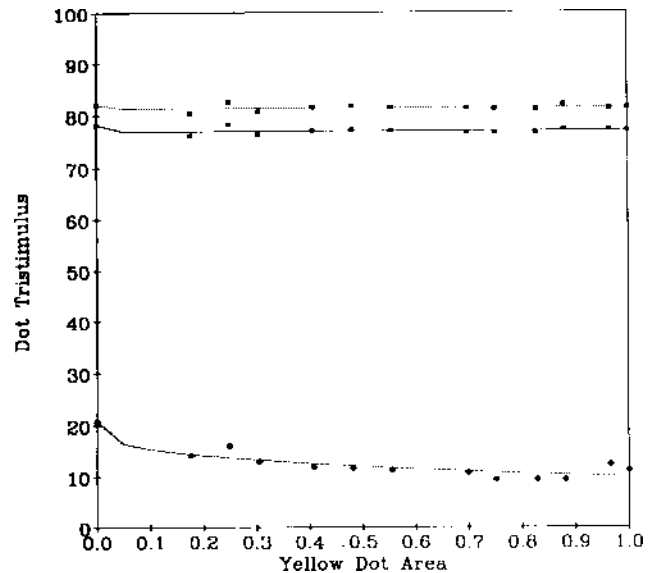


Figure 6. CIE X, Y, and Z TSVs for the yellow dots as a function of printed fractional area. The dot \equiv X, the square \equiv Y, and the diamond \equiv Z. The lines through the points are model predictions.

An additional perspective of the color mixing is shown by the CIE $L^*a^*b^*$ plot of the three colorants in Fig. 8. The scatter of the a^*b^* values, particularly for the dots, is due to the spatial fluctuations in the colorant layer uniformity. In the dots the paper fibers were clearly visible, and attempts were made to avoid measuring unrepresentative areas, but the scatter shows that this strategy was not completely successful. Except for the yellow colorant, the change in dot microtristimulus value with changing area is not so clear cut. Maing and colleagues¹¹ attempted to correct for the dot OD changes in ink-jet image by incorporation into the Y-N Eq. 2, but they were only partially successful. This correction was probably unsuccessful because of the small change in dot reflectance compared with the larger changes in paper reflectance with printed area.

Paper and Dot Tristimulus Modeling

From a practical perspective, factors for varying paper and dot micro-TSVs need to be incorporated into a new

half-tone model for accurate prediction of the micro-TSVs of the cyan, magenta, and yellow half-tone patches.

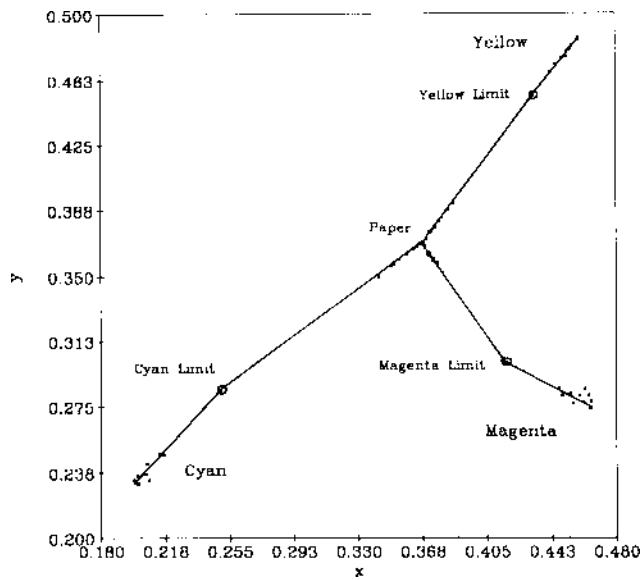


Figure 7. CIE chromaticity coordinates of the paper between the dots and the dots for cyan, magenta, and yellow colorants. The center of the diagram is the chromaticity of the white paper. The common point of the two line segments is the limiting value of the dot and the paper between the dots.

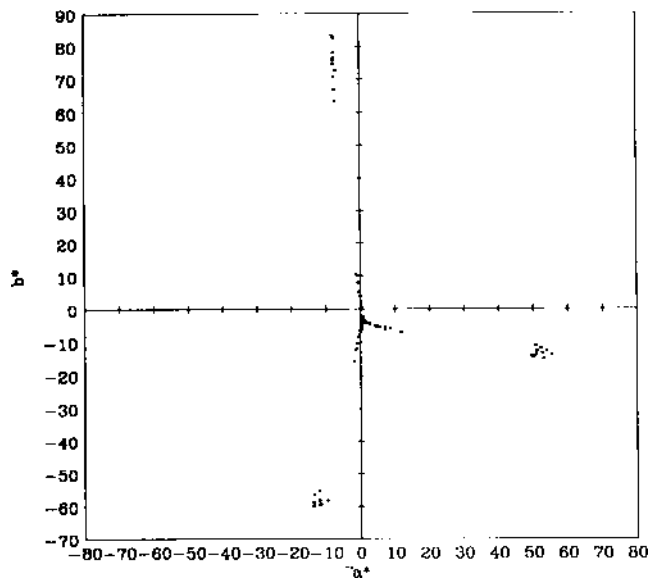


Figure 8. A CIE $L^*a^*b^*$ plot of the paper between the dots and the dots for cyan, magenta, and yellow colorants. The center of the diagram is the cool-white fluorescent illuminant.

The observation that both the paper microtristimulus values and the dot microtristimulus values appear to be smooth functions of printed dot area suggests that a simple representation may be successful. In keeping with a long tradition, a power function representation was selected. In the power function model, as the exponents go to zero the effect of the light scattering disappears. This and other power function forms were evaluated, but

there were not sufficient data to force any specific choice among the alternatives. The relationship between the paper and dot micro-TSVs is formalized in Eqs. 3(a) and 3(b), where T represents the X , Y , or Z TSV and $area$ equals the fractional area covered. T_{limit} is the limiting TSV for half-tone “holes” or dots, and p equals the power or exponent.

$$T_{paper}(area) = (T_{paper} - T_{limit})(1 - area)^p + T_{limit} \quad (3a)$$

$$T_{dot}(area) = T_{limit} - (T_{limit} - T_{solid})area^p \quad (3b)$$

In practice, only the exponent, p , in these equations is not measurable. All other values can be determined from spectral reflectance and transmittance data.

Nonlinear least-squares techniques were used to fit Eqs. 3(a) and 3(b) to the data points in Figs. 1-6. The results of these fits are represented by the lines in these figures. The parameters fitted to Eqs. 3(a) and 3(b) are listed in Table I. This simple model for the paper and dot micro TSVs does a good job of characterizing the change of these values with printed area.

The value of the exponent, p , for paper between the dots ranges from 0.264 to 0.392, with an average of 0.344. This exponent is the only parameter available that can capture the complex interaction between the spatial extent of the paper spread function, the dot-fill sequence within the half-tone cell, and the half-tone cell spatial frequency (ruling). The exact relationship of p with the above factors, and whether it should be constant for all colorants, is unknown. The lack of strong wavelength dependence of light scatter within paper (it is white) suggests that the p values could be estimates of a single value for the particular paper and printing conditions used in this experiment.

The dot exponent varies from 10^{-13} to 0.401. The very low exponents occur when there is little or no variation in the dot TSVs with area, as was observed for the yellow.

Half-tone Model

In the final analysis the prediction of the micro TSVs of the printed half-tone image is of prime importance. It appears that errors in the predicted half-tone reflectance using Eq. 1 can be attributed to the paper and dot TSVs that vary with the area of colorant on the paper because of light scattering within the paper. To test this hypothesis, a new half-tone model was formulated along the lines of Eq. 1, modified to include the functions for paper and dot tristimulus variation. Equation 4 represents the new model.

$$T_{half-tone} = T_{paper}(area) \times (1 - area) + T_{dot}(area) \times (area), \quad (4)$$

where the two functions, $T_{paper}(area)$ and $T_{dot}(area)$, are given by Eqs. 3(a) and 3(b), and $T_{half-tone}$ represents the X , Y , or Z TSV of the half-tone tint.

The macrospectral reflectances of a series of 16 half-tone tints, consisting of 1-cm squares of cyan, magenta, and yellow colorants, were measured. The nominal fractional dot area increment between the patches was 1/16. CIE TSVs for cool-white fluorescent were calculated

from the halftone tint macrospectral data. Figures 9-11 illustrate the results of using Eq. 4, with the parameters listed in Table I, to predict the patch TSVs. One exception was yellow. It was discovered after the measurement apparatus had been taken apart that the reflectance reference had drifted during the large-area halftone measurements. To account for this drift a factor of approximately 0.95 was used to scale the model results. The CIE $L^*a^*b^*$ color difference metric was used as the measure of goodness of fit, and results are summarized in Table II.

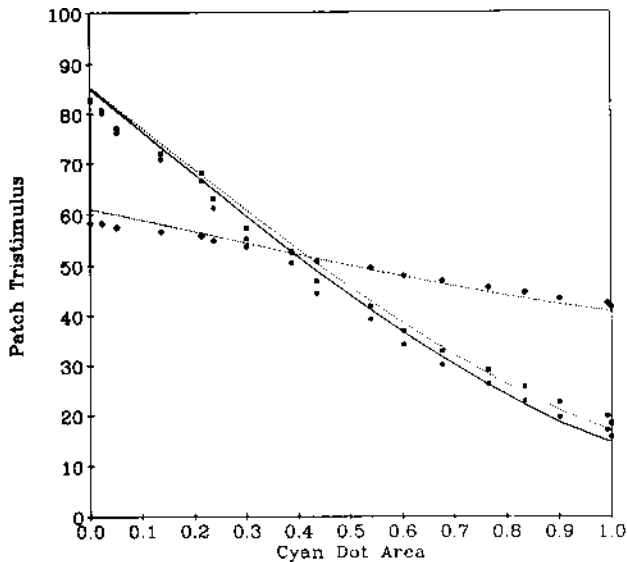


Figure 9. Measured and predicted CIE TSVs of the 1-cm-square cyan halftone tints as a function of printed fractional area. The dot \equiv X, the square \equiv Y, and the diamond \equiv Z. The lines through the points are model predictions.

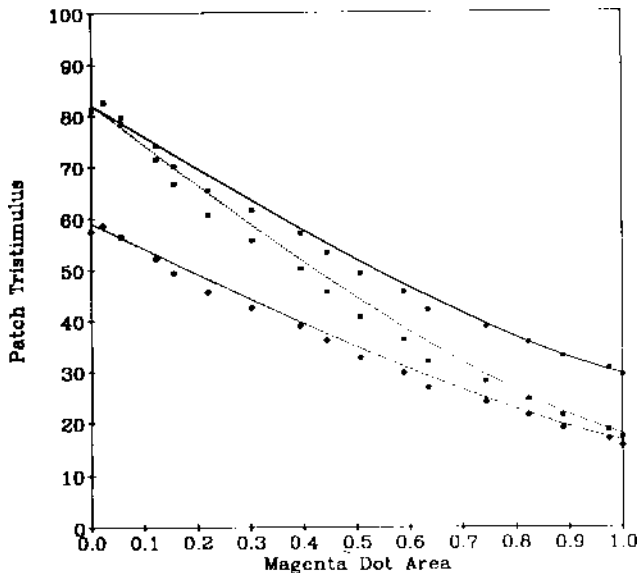


Figure 10. Measured and predicted CIE TSVs of the 1-cm-square magenta halftone tints as a function of printed fractional area. The dot \equiv X, the square \equiv Y, and the diamond \equiv Z. The lines through the points are model predictions.

When this particular printer was tested for spatial repeatability the average color difference was about 5, showing that the results of the modified halftone model are quite good.

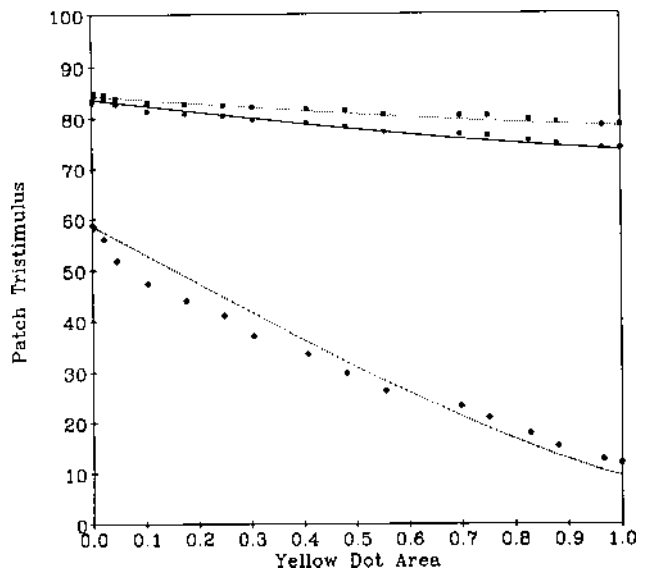


Figure 11. Measured and predicted CIE TSVs of the 1-cm-square yellow halftone tints as a function of printed fractional area. The dot \equiv X, the square \equiv Y, and the diamond \equiv Z. The lines through the points are model predictions.

TABLE II. Halftone Model Performance Summary in Terms of Average CIE $L^*a^*b^*$ Color Difference and Maximum Color Difference for Cyan, Magenta, and Yellow Halftone Images

Halftone color	CIE $L^*a^*b^*$ color difference	
	Average	Maximum
Cyan	2.95	4.81
Magenta	2.95	6.15
Yellow	4.49	8.37

Conclusions

The change in the paper micro-TSVs as a function of the fractional dot area printed was significant. A simple power function model was found to be adequate to characterize the paper and dot TSVs as a function of printed fractional area. The exponents required to account for light scattering in paper between the dots were approximately 0.33 and depended on the colorant and the X, Y, and Z TSV. They will also depend on the halftone cell geometry, halftone spatial frequency, and the extent of the light scatter within the paper.

Dot TSVs did not change as much with area as did the paper TSV. Dot TSV exponents varied from almost zero to 0.401. These very low powers occurred when there was only a very small change in the dot TSVs with area.

The color of the paper between single-colorant halftone dots printed by a wax thermal transfer printer is a mixture of the base paper micro-TSVs and the limiting value determined by the TSV of the colorant microspectral transmittance and the paper spectral reflectance product. Dot colors, for very small dot areas, are a linear mixture of the same limiting color and the solid color. These observations suggest that the simple Y-N n factor correction cannot, in principle, be correct because it assumes that these quantities are constant.

The CIE $L^*a^*b^*$ color difference for single-color halftone patches, using these relationships to predict the average TSVs, ranged from about 2.95 to 4.49. The maximum color difference was less than 8.4 and within the range of the printer spatial repeatability.

With the caveat that only single colors were measured in this study, recently reported color difference results using variations in the Neugebauer equations^{8,20} and other models,²⁰ suggest that the proposed model may give better performance when extended to three or four colors.

Extending and validating the model for three- and four-color halftone systems and finding simpler methods to determine the parameters must be done before these results can be applied practically.

References

1. M. Bruno, Ed., *Pocket Pal*. 50th ed., International Paper Co., New York, 1983.
 2. A. Murray, *J. Franklin Inst.* **221**, 721 (1936).
 3. J. A. C. Yule and W. J. Neilsen, *Tech. Assn. Graphic Arts (TAGA) Proc.*, 1951, p. 65.
 4. M. Pearson, *TAGA Proc.*, 1980, p. 415.
 5. H. E. J. Neugebauer, *Z. Tech. Phys.* **36**: 75 (1937).
 6. P. G. Engeldrum, *J. Imaging Technol.* **12**: 26 (1986).
 7. S. Yoshinobu and T. Mizuno, *J. Imaging Sci. Technol.* **37**: 385 (1993).
 8. R. Rolleston and B. Balasubramanian, *Proc. of IS&T/SID Color Imaging Conference*, 1993, p. 32.
 9. I. Pobboravsky and M. Pearson, *TAGA Proc.*, 1972, p. 65.
 10. J. A. S. Viggiano, *TAGA Proc.*, 1985, p. 647.
 11. W. Maing, Y. Miyake, N. Abe, and S. Kubo, *J. Imaging Technol.* **14**: 6 (1988).
 12. F. P. Callahan, *J. Opt. Soc. Amer.* **42**: 104 (1952).
 13. D. R. Lehmbek, in *SPSE's 28th Annual Conference and Seminar on Quality Control*, SPSE (now IS&T), Springfield, VA, 1975, p. 155.
 14. F. Ruckdeschel and O. G. Hauser, *Applied Optics* **17**: 3376 (1978).
 15. M. Maltz, *J. Appl. Photogr. Eng.* **9**: 83 (1983).
 16. J. A. C. Yule, D. J. Howe, and J. H. Altman, *TAPPI* **50**: 337 (1967).
 17. F. R. Clapper and J. A. C. Yule, *J. Opt. Soc. Amer.* **43**: 600 (1953).
 18. P. Oittinen and H. Saarelma, *TAPPI* **65**: 47 (1982).
 19. W. D. Wright, *The Measurement of Colour*, Hilger & Watts, Ltd., London, 1958, p. 73.
 20. H. R. Kang, *Proc. of IS&T/SID Color Imaging Conference*, 1993, p. 78.
- * Previously published in the *Journal of Imaging Science and Technology*, **38**(6) pp. 545–551, 1994.